Analytical Methods

Accepted Manuscript

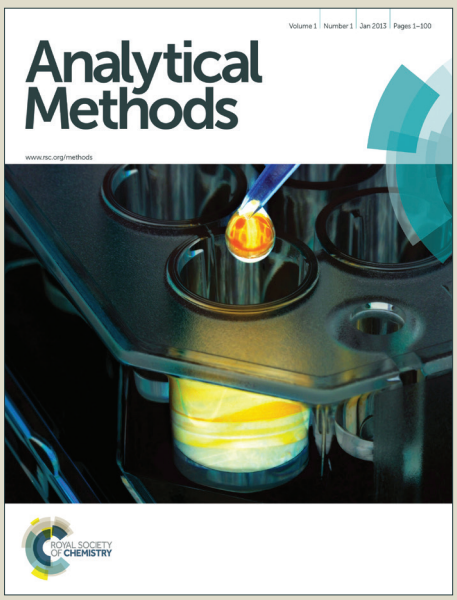

ROYAL SOCIETY OF CHEMISTRY

www.rsc.org/methods

Journal Name

RSCPublishing

COMMUNICATION

Direct Imaging of Single Gold Nanoparticle Etching: Sensitive Detection of Lead Ions

Cite this: DOI: 10.1039/x0xx00000x

Dinggui Dai, Dong Xu, Xiaodong Cheng and Yan He*

Received 00th January 2012,
Accepted 00th January 2012

DOI: 10.1039/x0xx00000x

www.rsc.org/

We present a highly sensitive Pb^{2+} detection method by in-situ real-time imaging of Pb^{2+} catalyzed etching and size reduction of immobilized single gold nanoparticles with darkfield microscopy. The detection limit is 0.2 pM, suggesting direct observation of the catalytic activity of ~ 5 lead ions on one gold nanoparticle surface.

Lead ions, one of the most toxic metallic pollutions, have become a tremendous threat to human health.[1] Once Pb^{2+} is into human body, it is hard to get excreted, and high concentration of Pb^{2+} could impede the circulation and update of blood, causing headache, dizziness, fatigue or even brain damage.[2] Because of its high toxicity and wide spread in aquatic ecosystem, accurate detection of Pb^{2+} at low concentration is very important. Over the past decades, sensitive and reliable instrumentation techniques based on atomic absorption spectrometry (AAS),[3] inductive coupled plasma mass spectrometry (ICP-MS),[4] X-ray fluorescence spectroscopy[5] and inductive coupled plasma atomic emission spectrometry (ICP-AES)[6] have been established for Pb^{2+} detection. Some new analytical methods using specialized probes based on chromophores,[7] DNAzymes,[8] fluorophores,[9] oligonucleotides[10] or nanoparticles[11] have also been developed for Pb^{2+} sensing during recent years. For instance, Liu et al. designed a highly sensitive and selective colorimetric sensor by using Pb^{2+}-dependent DNAzyme as a target recognition element and DNA-functionalized gold nanoparticles as a detection sensor.[12] Huang and co-workers reported a sensitive and cost-effective colorimetric assay based on the fact that Pb^{2+} would accelerate the etching rate of gold in the ammoniacal $S_2O_3^{2-}$ system.[13]

Owing to their unique optical and chemical properties including size, shape and environment dependent localized surface plasmon resonance (LSPR) spectra, mild surface chemistry and low biotoxicity, gold nanoparticles (AuNPs) have been utilized in diverse areas as chemical or biological sensors, particularly in the field of single particle detection (SPD).[14] SPD represents the ultimately sensitive detection without any target or signal amplification,[15] and single AuNPs can serve as non-fluorescence SPD probes due to their large LSPR absorption and scattering cross sections and high photostability.[16] For example, by using dark field microscopy (DFM), Xiao presented a single molecule detection method for DNA sensing using colour coded single plasmonic nanoparticles and reached a detection limit of 0.02 pM.[17] Xiong and co-workers demonstrated highly sensitive sulphide detection in living cell on the basis of single-particle spectral imaging with AuNR-Ag core-shell nanoparticles as probes.[18] Long group reported a dark-field microscopy-based method, involving NADH-mediated reduction of Cu^{2+} onto AuNPs to form Au@Cu nanoparticles, to detect NADH activity at single particle level inside cells and monitored the effect of anticancer drugs on the cell metabolism.[19]

In this study, by using DFM-based detection of single AuNP scattering intensity, a highly sensitive method for Pb^{2+} sensing was proposed. Figure S1 shows the schematic diagram of the reaction. Different from other target-induced AuNP aggregation-based colorimetric assays, this method took advantages of Pb^{2+} induced AuNP size variation. When Pb^{2+} was added into the mixture of $S_2O_3^{2-}$, 2-mercaptoethanol (2-ME) and AuNPs, the Pb-Au complexes accelerated AuNPs dissolving into solution and their size reduction, leading to a sharp decrease in the LSPR scattering intensity of the AuNPs with little spectral shift. The fact that an individual AuNP can act as a probe for sensitive detection of Pb^{2+} allows miniaturization of the sensing system and significant reduction of sample volume. As a result, Pb^{2+} concentration in homogenous solution was able to be determined as sensitive as 0.2 pM. Further calculation indicated that we were actually detecting the catalytic activity of just ~ 5 Pb^{2+} ions on one AuNP surface when the Pb^{2+} concentration was 0.2 pM. To our knowledge, this is the first time to use a non-fluorescence SPD technique for lead ion detection. This approach could be further applied to study real-time single molecule reaction kinetics and catalytic mechanisms.

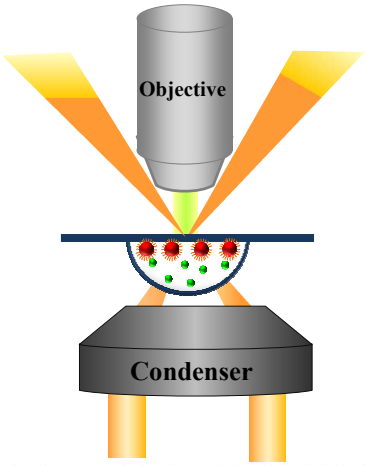

Figure 1. Schematic diagram of single particle dark field microscopy.

The optical setup is shown in Figure 1. According to previous reports, the smaller the AuNP size, the higher the sensitivity. But due to the limited sensitivity of our CCD camera (see discussions below), it is hard to obtain enough signal-to-noise ratio if the diameter of AuNPs is smaller than 30 nm. Therefore, we chose AuNPs of average size 50.6 ± 6.7 nm (Figure S2A) for this SPD assay. The classical etching experiment was performed to test whether the etching reaction could happen when using these large AuNPs. As shown in Figure 2, the absorbance of the AuNP solution at 533 nm decreased dramatically with Pb^{2+} concentration increasing from 0.5 nM to 50 μM.

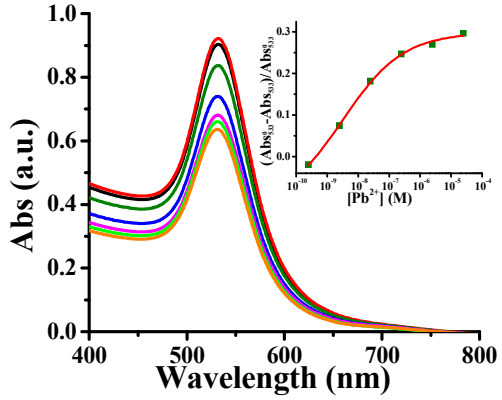

Figure 2. UV-Vis absorption spectra of 2-ME/$S_2O_3^{2-}$/AuNPs in response to Pb^{2+} concentrations ranging from 500 pM~50 μM in bulk solution. The insert shows the ratio (A^0_{533}-A_{533})/A^0_{533} as a function of the concentration of Pb^{2+}.

Subsequently, we tested the selectivity of the nanoprobes toward Pb^{2+} for a wide range of biologically and environmentally relevant metal ions including (Fe^{3+}, Co^{2+}, Cu^{2+}, Cd^{2+}, Ni^{+}, Zn^{2+}, Al^{3+}, Na^{+}, Mg^{2+} (5 μM)), and Pb^{2+} (5 nM), Figure S3 shows that the probes responded selectively toward Pb^{2+} ions by a factor of 100 or more relative to other metal ions. Taken the above data together, the 50 nm AuNPs can be used for highly sensitive and selective Pb^{2+} detection.

As demonstrated in previous reports by others, the scattering intensity of AuNPs is highly sensitive to their size.[20] According to the Mie theory, the scattering cross section σ_{sca} of an AuNP can be described by[21]

$$\sigma_{sca} = \frac{24\pi^3 V^2}{\lambda^4}\left[\frac{\varepsilon(\lambda)-\varepsilon_m}{\varepsilon(\lambda)+2\varepsilon_m}\right]^2$$

Where λ is the wavelength of the light, V is the volume of the AuNP, and ε(λ) and ε_m are the permittivities of the AuNP and surrounding environment, respectively. The equation shows that the scattering intensity of AuNP is proportional to the square of its volume.

Figure 3A and 3B present the calculated scattering spectra and the simulated colour scattering images of 4 different sizes of AuNPs from 30 nm to 60 nm. It can be seen that, when the size of the AuNP doubles from 30 nm to 60 nm, both its intensity and color/spectrum vary a lot, suggesting that single AuNP aggregation-based assays can be detected using either intensity or colorimetric/spectral sensing. When the size of AuNP reduces from 50 nm to 30 nm, there is a significant decrease in AuNP scattering intensity, but the AuNP colour remains largely green. Thus, Pb^{2+} induced single AuNP etching and size reduction should be more efficiently detected by the change of AuNP scattering intensity. Figure 3C shows the quantitative relationship between the AuNP size and intensity. There is 88% intensity decrease when the particle reduces from 50 nm to 30 nm.

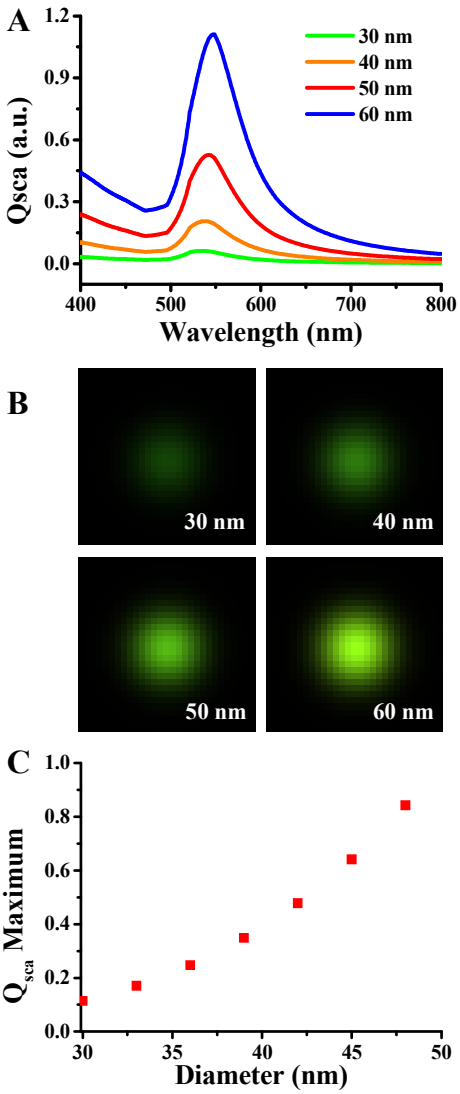

Figure 3. (A) Simulated scattering spectra and (B) Calculated dark field scattering images of 30, 40, 50 and 60 nm AuNPs according to the Mie theory. (C) Normalized scattering intensity maximum as a function of AuNP diameter.

Before performing the SPD assay, the signal-to-noise ratio (S/N) of the optical system needs to be optimized, which is affected by both the ISO level and the exposure time of the CCD camera. Figure S4 shows the S/N results obtained from a blank AuNP sample with different camera settings. The highest S/N was reached when we set the ISO level to 200 and the exposure time to 3 s. Next, we evaluated the stability of the single particle measurement by monitoring the time-dependent variation of AuNP intensity. It can be seen in Figure S5 that the fluctuation of the unreacted AuNPs was ~ 5% within 6 h. Therefore, AuNP intensity decreased over 5% can only result from etching reactions. Third, we must take into account the stability of the reaction system. It is known that $Na_2S_2O_3$ could readily decompose into SO_2 and Na_2SO_4 in air, which could hinder the formation of $Au(S_2O_3)^{3-}$ complexes and slow down the AuNP etching rate if the $Na_2S_2O_3$ concentration becomes too low. To alleviate this problem, we had the reactions occur in a 40 µl air-tight cell created by gluing the coverslip and a concave glass slide together with nail polish. According to the chemical reaction equation ($4Au + O_2 + 2H_2O + 8S_2O_3^{2-} \rightarrow 4Au(S_2O_3)_2^{3-} + 4OH^-$), the dissolved O_2 (solubility 0.25 mM/L) in this 40 µl solution is far more than sufficient for the etching reaction at room temperature of 25°C. This sealed micro chamber also prevents evaporation of the solution. Finally, to prove that the Pb^{2+} induced reaction could actually happen and be observed at the single particle level under DFM, 2 nM Pb^{2+} solution with 2-ME was added into such a reaction system and monitored under DFM for 6 h. As shown in Figure S6, the scattering intensity of singe AuNPs decreased rapidly initially and then slowed down after 6 h, indicating the single-particle-based etching reaction did occur and completed in about 6 h. Figure 4 displays typical DFM images of the single AuNPs before and after reacting with Pb^{2+}, there was an apparent decrease in AuNP intensity after the reaction. And the TEM results (Figure S2) suggested that the final size of the AuNPs declined for nearly 5 nm.

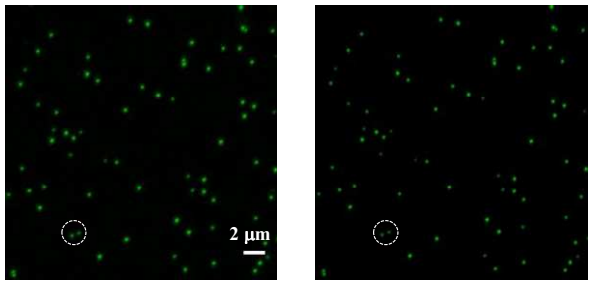

Figure 4. Typical AuNP dark field images (A) before and (B) after reacting with 2 nM Pb^{2+}.

To find out the performance of this single particle detection method for quantitative Pb^{2+} sensing, we performed a series of experiments with various Pb^{2+} concentrations, $[Pb^{2+}]$. Immobilized single $S_2O_3^{2-}$/AuNPs probes were immersed in the Pb^{2+} solution for 6 h and their beginning and end DFM images were recorded, respectively. To investigate the sensitivity and dynamic range, over 50 nanoprobes were randomly selected at each $[Pb^{2+}]$, and the resulting $\Delta I/I_0$ values were recorded and calculated. We use the intensity ratio, which compares the intensity variation to the original intensity value of each AuNPs, to eliminate the factor of AuNP size difference and get more reliable and precise results. By Gaussian fitting their distributions, the average $\Delta I/I_0$ value at each $[Pb^{2+}]$ (Figure 5A) as well as their dependence on $[Pb^{2+}]$ (Figure 5B) was obtained. The limit of detection was found to be 0.2 pM, the lowest in all Pb^{2+} sensing assays as far as we know. With increasing $[Pb^{2+}]$, $\Delta I/I_0$ value scaled up roughly linearly with the logarithm of $[Pb^{2+}]$ from 0.2 pM to 200 pM, but started to level off at higher $[Pb^{2+}]$, indicating that the dynamic range of this assay was not very large. This is attributed to that the activity sites for Pb^{2+} adsorption on each single AuNP probe surface were limited in number and they were all occupied when $[Pb^{2+}]$ was too large, hindering further acceleration of the etching rate.

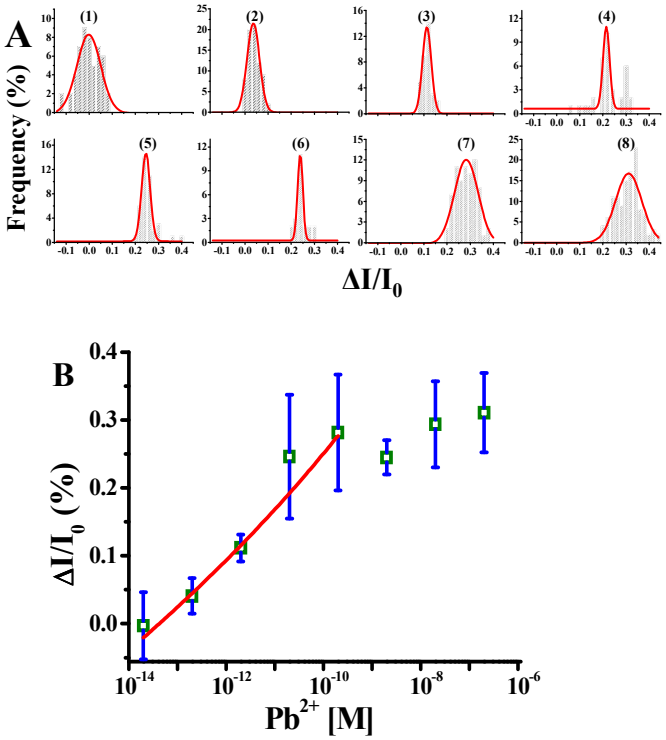

Figure 5. (A) Distribution of $\Delta I/I_0$ after adding (1) 0 pM, (2) 0.2 pM, (3) 2 pM, (4) 20 pM, (5) 200 pM, (6) 2 nM, (7) 20 nM, (8) 200 nM Pb^{2+}. Over 50 particles were counted in each case. (B) Calculated $\Delta I/I_0$ values from the dark field images as a function of Pb^{2+} concentration. (The first point represents the blank).

Besides ultrasensitive quantification of the concentration of Pb^{2+}, we can also get additional mechanistic insights on the Pb^{2+} catalyzed AuNP etching reaction at the single particle level. By statistical analysis of the number of immobilized single AuNPs observed during darkfield imaging, we estimated that each image containing ~180 nanoprobes. From the image size (1360 × 1024 pixels), the pixel size (6.45 µm) and the magnification of the objective (40 ×), it can be calculated that the sample area corresponding to each image is 3.6×10^{-8} m^2. According to the size of the air-tight concavity (d = 15 mm and area = 1.78×10^{-4} m^2), there is roughly 8.8×10^5 immobilized AuNPs enclosed in the reaction chamber. Assuming all Pb^{2+} ions in the 40 µL solution were adsorbed onto the surface of AuNPs when the Pb^{2+} concentration is very low, there will be in average only ~ 5 Pb^{2+} ions adsorbed onto every AuNP surface when $[Pb^{2+}]$ = 0.2 pM. In other word, at this concentration, we were monitoring not only the intensity change of single AuNPs, but also the catalytic behaviors of just a few Pb^{2+} ions. To our knowledge, this is the first report on real time catalysis reaction studies at nearly single ion level. On the other hand, from the turning point of the $\Delta I/I_0$ vs $\log([Pb^{2+}])$ curve in Figure 5B, we can determine that on each AuNP surface, the maximum number of active sites is ~ 5,000 or there are about 0.6 ~ 1.0 active sites per nm^2. Further studies along this line could provide more information.

In conclusion, by using DFM and single 50 nm AuNPs as the probes, we have studied Pb^{2+} catalyzed AuNP etching reactions at the single particle level. Since the LSPR scattering intensity of AuNPs is highly sensitive to their size and topography change, this method is able to detect as a low as 0.2 pM Pb^{2+} in the solution or in average the catalytic behaviors of ~ 5 Pb^{2+} ions on an AuNP surface. Similar approaches could be developed for ultrasensitive detection of other heavy metal ions or small molecules and for single particle catalysis mechanism studies.

This work was supported by NSFC 21127009, NSFC 91027037, and Hunan University 985 fund.

Notes and references

State Key Laboratory of Chemo/Biosensing and Chemometrics, College of Chemistry and Chemical Engineering, College of Biology, Hunan University, Changsha, 410082, P. R. China. yanhe2021@gmail.com

†Electronic Supplementary Information (ESI) available: [Experimental details and additional Figure S1-6]. See DOI: 10.1039/c000000x/

1. (a)M. Ahamed, M. Kaleem and J. Siddiqui, *Clin. Nutr.*, 2007, **26**, 400-408; (b)N. Healey, *Radiat. Prot. Dosim.*, 2009, **134**, 143-151; (c)H. L. Needleman, *Human lead exposure*, CRC Press, 1992.
2. (a)A. M. Ronco, Y. Gutierrez, N. Gras, L. Muñoz, G. Salazar and M. N. Llanos, *Biol. Trace. Elem. Res.*, 2010, **136**, 269-278; (b)J. F. Rosen, *Toxicology*, 1995, **97**, 11-17.
3. M. Ghaedi, A. Shokrollahi, K. Niknam, E. Niknam, A. Najibi and M. Soylak, *J. Hazard. Mater.*, 2009, **168**, 1022-1027.
4. A. Michalska, M. Wojciechowski, B. Wagner, E. Bulska and K. Maksymiuk, *Anal. Chem.*, 2006, **78**, 5584-5589.
5. D. Vantelon, A. Lanzirotti, A. C. Scheinost and R. Kretzschmar, *Environ. Sci. Technol.*, 2005, **39**, 4808-4815.
6. D. D. Afonso, S. Baytak and Z. Arslan, *J. Anal. At. Spectrom.*, 2010, **25**, 726-729.
7. (a)P. Narkwiboonwong, G. Tumcharern, A. Potisatityuenyong, S. Wacharasindhu and M. Sukwattanasinitt, *Talanta.*, 2011, **83**, 872-878; (b)E. Ranyuk, C. M. Douaihy, A. Bessmertnykh, F. Denat, A. Averin, I. Beletskaya and R. Guilard, *Org. Lett.*, 2009, **11**, 987-990; (c)Z. Yuan, M. Peng, Y. He and E. S. Yeung, *Chem. Commun.*, 2011, **47**, 11981-11983.
8. (a)L. Zhang, B. Han, T. Li and E. Wang, *Chem. Commun.*, 2011, **47**, 3099-3101; (b)Y. Wen, C. Peng, D. Li, L. Zhuo, S. He, L. Wang, Q. Huang, Q.-H. Xu and C. Fan, *Chem. Commun.*, 2011, **47**, 6278-6280; (c)Z. Wang, J. H. Lee and Y. Lu, *Adv. Mater.*, 2008, **20**, 3263-3267; (d)J. Liu and Y. Lu, *J. Am. Chem. Soc.*, 2003, **125**, 6642-6643.
9. (a)P. Chen, B. Greenberg, S. Taghavi, C. Romano, D. van der Lelie and C. He, *Angew. Chem.*, 2005, **117**, 2775-2779; (b)I.-B. Kim, A. Dunkhorst, J. Gilbert and U. H. Bunz, *Macromolecules.*, 2005, **38**, 4560-4562; (c)S. Deo and H. A. Godwin, *J. Am. Chem. Soc.*, 2000, **122**, 174-175; (d)C.-T. Chen and W.-P. Huang, *J. Am. Chem. Soc.*, 2002, **124**, 6246-6247; (e)J. Y. Kwon, Y. J. Jang, Y. J. Lee, K. M. Kim, M. S. Seo, W. Nam and J. Yoon, *J. Am. Chem. Soc.*, 2005, **127**, 10107-10111.
10. (a)L. Movileanu, S. Howorka, O. Braha and H. Bayley, *Nat. Biotechnol.*, 2000, **18**, 1091-1095; (b)S. Howorka, S. Cheley and H. Bayley, *Nat. Biotechnol.*, 2001, **19**, 636-639.
11. (a)Y. Kim, R. C. Johnson and J. T. Hupp, *Nano lett.*, 2001, **1**, 165-167; (b)J.-T. Zhang, L. Wang, J. Luo, A. Tikhonov, N. Kornienko and S. A. Asher, *J. Am. Chem. Soc.*, 2011, **133**, 9152-9155; (c)K. Yoosaf, B. I. Ipe, C. H. Suresh and K. G. Thomas, *The Journal of Physical Chemistry C*, 2007, **111**, 12839-12847; (d)C.-I. Wang, C.-C. Huang, Y.-W. Lin, W.-T. Chen and H.-T. Chang, *Anal. Chim. Acta*, 2012, **745**, 124-130.
12. J. Liu and Y. Lu, *J. Am. Chem. Soc.*, 2005, **127**, 12677-12683.
13. Y.-L. Hung, T.-M. Hsiung, Y.-Y. Chen and C.-C. Huang, *Talanta.*, 2010, **82**, 516-522.
14. (a)J. Yu, J. Xiao, X. Ren, K. Lao and X. S. Xie, *Science.*, 2006, **311**, 1600-1603; (b)B. Huang, H. Wu, D. Bhaya, A. Grossman, S. Granier, B. K. Kobilka and R. N. Zare, *Science.*, 2007, **315**, 81-84; (c)A. Agrawal, C. Zhang, T. Byassee, R. A. Tripp and S. Nie, *Anal. Chem.*, 2006, **78**, 1061-1070.
15. (a)W. Moerner and M. Orrit, *Science.*, 1999, **283**, 1670-1676; (b)E. S. Yeung, *Annu. Rev. Phys. Chem.*, 2004, **55**, 97-126; (c)X. S. Xie and J. K. Trautman, *Annu. Rev. Phys. Chem.*, 1998, **49**, 441-480; (d)J.-Y. Lee, J. Li and E. S. Yeung, *Anal. Chem.*, 2007, **79**, 8083-8089.
16. (a)S. Berciaud, L. Cognet, P. Tamarat and B. Lounis, *Nano lett.*, 2005, **5**, 515-518; (b)K. L. Kelly, E. Coronado, L. L. Zhao and G. C. Schatz, *J. Phys. Chem. C.*, 2003, **107**, 668-677; (c)W. Haiss, N. T. Thanh, J. Aveyard and D. G. Fernig, *Anal. Chem.*, 2007, **79**, 4215-4221.
17. L. Xiao, L. Wei, Y. He and E. S. Yeung, *Anal. Chem.*, 2010, **82**, 6308-6314.
18. B. Xiong, R. Zhou, J. Hao, Y. Jia, Y. He and E. S. Yeung, *Nat. Commun.*, 2013, **4**, 1708.
19. L. Zhang, Y. Li, D. W. Li, C. Jing, X. Chen, M. Lv, Q. Huang, Y. T. Long and I. Willner, *Angew. Chem.*, 2011, **123**, 6921-6924.
20. (a)S. Link and M. A. El-Sayed, *Int. Rev. Phys. Chem.*, 2000, **19**, 409-453; (b)C. Jing, Z. Gu, Y.-L. Ying, D.-W. Li, L. Zhang and Y.-T. Long, *Anal. Chem.*, 2012, **84**, 4284-4291.
21. G. Mie, *Ann. Phys-berlin.*, 1908, **330**, 377-445.

Table of contents